

Downhill Energy Transfer via Ordered Multichromophores in Light-Harvesting Capsules

Zhifei Dai,* Lars Dähne, Edwin Donath,[†] and Helmuth Möhwald

Max-Planck Institute of Colloids and Interfaces, D-14424 Golm/Potsdam, Germany

Received: February 16, 2002; In Final Form: August 25, 2002

A variety of light-harvesting capsules were successfully constructed by assembling polyelectrolyte complexes and antenna dyes of graduated absorption energy into nanoscale walls (thickness of a single layer around 2 nm). Two-step downhill energy transfer was demonstrated with absorption and fluorescence spectroscopy for the first time on light-harvesting capsules. Energy transfer occurs parallel to the capsule surface if the dyes are coadsorbed to the preassembled capsule wall. Energy transfer perpendicular to the surface was achieved by sequentially assembling the dyes in different layers of the wall. Although perpendicular energy transfer is less efficient because of longer intermolecular distances, utilization of J-aggregates and optimization of dye combinations and dye ratios yielded an efficient energy cascade along three components. The light-harvesting capsules are analogous to the light reactions of photosynthesis in chloroplasts.

Introduction

Photosynthetic light-harvesting complexes consist of up to hundreds of pigments organized in elaborate 3D structures, and the light reactions of photosynthesis occur in closely coupled pigment systems.^{1,2} Light energy is absorbed over a wide spectral range by a network of so-called antenna pigment–proteins and is very efficiently funneled through unidirectional energy transfer toward the photochemical reaction center (RC) where the energy is converted through a sequence of electron-transfer reactions.³ The juxtaposition of chromophores tunes their electronic interactions, which govern both their absorptive/emissive properties and the kinetics of energy transfer.⁴ In the purple bacteria photosynthetic unit, the excitation dynamics was described as a sequence of transfer steps between distinct spectral bands, B800 → B850 → B880 → RC.² The ability to design and construct molecular architectures in which the flow of excited-state energy can be directed in a controlled manner, as occurs in the photosynthetic unit, is expected to have substantial applications in solar energy conversion, optoelectronics, photonics, and other areas of nanotechnology.⁵

The approach for meeting the challenge of organizing a large number of pigments is to design small- or medium-sized multichromophoric arrays that self-assemble into light-harvesting architectures. One strategy to mimic this type of behavior involves the covalent linkage of chromophores, but the synthesis becomes very demanding for the increasing complexity of such systems as more chromophores are added.⁶ Simpler self-organization processes used in the layer-by-layer self-assembly (LbL) technique of oppositely charged polyelectrolytes permit the construction of nanoscale devices and semibiological hybrids in planar films or spherical objects.⁷ Numerous studies have been performed on polyelectrolyte (PE) capsules prepared by means of this method.⁸ Recently, functional dyes were introduced into capsules as noncovalently linked guest molecules by a variation of the LbL technique. Different components can be assembled within one layer or along the radial direction.⁹

As one example of this hybrid approach, we prepared shape-persistent spherical hollow capsules with noncovalently linked multichromophores and polyelectrolytes with a cavity diameter of $\sim 4\ \mu\text{m}$, which are called light-harvesting capsules (LHCap). The motivation for preparing multichromophoric arrays is to study and ultimately control the energy-transfer direction. For their final application in light-harvesting antenna systems, spherical devices with large photosensitive surface areas and redox-active cores have to be used in analogy to the chloroplasts in photosynthesis. The PE capsules have the potential for the construction of such advanced microspheres. By analogy to nature, light should be absorbed mainly at the outer surface of the capsules and transferred unidirectionally to the capsule interior. The interior can be filled by systems that can use the energy for subsequent reactions.

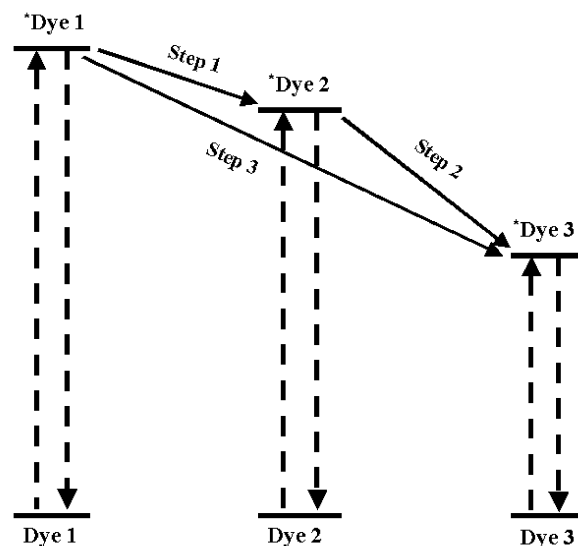
In the following sections, we will be concerned with various Förster resonance energy-transfer (FRET) steps and will examine in detail how light is absorbed by antenna pigments at the surface of capsules and how the energy is transferred to the capsule interior. In addition, we will combine the structure of capsules and dyes with the results of spectroscopic measurements relevant to energy transfer between complexes to construct models to advance our conceptual understanding of their interaction.

Experimental Section

To mimic the photosynthetic energy-transfer process, light-harvesting capsules (LHCap) were constructed with three dyes deposited into the wall of the capsule by means of a layer-by-layer self-assembly technique, wherein the excited-state energy levels decrease in the following order: dye 1 > dye 2 > dye 3. In general, the excitation dynamics in these systems can be described as the sequence of a three-component energy-transfer cascade between distinct spectral bands. Scheme 1 shows paths for the flow of excited-state energy in the constructed LHCap. We will see that the elementary processes are in fact much more complicated than this simple Scheme shows. The height of the lines in Scheme 1 indicates the relative excited-state energy level of the various components. Path 1 proceeds downhill in energy in a stepwise manner from dye 1 → dye 2 → dye 3; the transfer

* Corresponding author. E-mail: zhifei.dai@mpikg-golm.mpg.de. Tel: +49 331 567 9235. Fax: +49 331 567 9202.

[†] Leipzig University, Department of Medical Physics and Biophysics, D-04103 Leipzig, Germany.

SCHEME 1: Energy-Transfer Pathways for the Antenna System

from the nonadjacent dye 1 to dye 3 occurs via the intermediacy of dye 2. In path 2, energy is transferred directly from dye 1 to dye 3. There are two options for energy-transfer directions according to the dye arrangement, as shown in Scheme 2. One is parallel to the surface of the capsules with dyes coadsorbed to the preassembled (PSS/PAH)₄ hollow capsules. The other is perpendicular across the wall of the capsules with the dyes layered along the radial direction of the capsules. In both options, the excited-state energy of dye 1 rapidly reaches dye 3 via FRET in the shell. If the capsule interior contains a guest having an excited state of lower energy than that of dye 3, the energy can be transferred to the guest via a through-space process.

The structural formulas of the dyes used in this work are shown in Scheme 3. The dyes were selected with large spectral overlap between the donor emission and the acceptor absorption to achieve efficient FRET.¹⁰ 5-Chloro-2-[[5-chloro-3-(3-sulfopropyl)-3H-benzothiazol-2-ylidene]-methyl]-3-(3-sulfopropyl)-benzothiazolium hydroxide, inner salt, ammonium salt (TC) and 5-chloro-2-[2-[5-chloro-3-(3-sulfopropyl)-3H-benzothiazol-2-ylidene]-methyl]-but-1-enyl]-3-(3-sulfopropyl)-benzothiazolium hydroxide, inner salt, sodium salt (TCC) were obtained from FEW Chemicals GmbH, Germany. 10-Chloro-1,1'-di(3-sulfo-

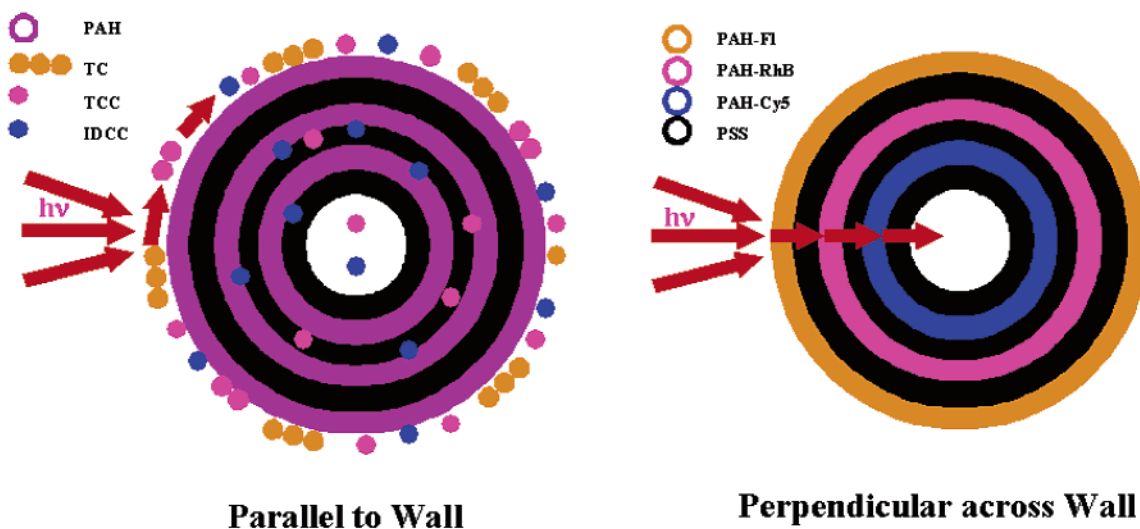
propyl)-3,3,3',3'-tetramethylindodicarbocyanine triethylammonium salt (IDCC) was synthesized according to the method reported.¹¹

Cyanines were chosen because much is known about their characteristic photophysical properties because of their extensive applications.¹² Sodium poly(styrene sulfonate) (PSS, $M_w \approx 70\,000$) and poly(allylamine hydrochloride) (PAH, $M_w \approx 70\,000$) were obtained from Aldrich. Melamine formaldehyde resin particles (MF) (4 μm) were obtained from Microparticles GmbH, Berlin, Germany. PAH was labeled with derivatives of fluorescein, rhodamine B, and indodicarbocyanine (expressed as PAH-FI, PAH-RhB, and PAH-Cy5, respectively) as reported.¹³ The degree of labeling was about 1 fluorescein molecule per 118 PAH units, 1 rhodamine molecule per 245 PAH units, and 1 cyanine molecule per 240 PAH units.

Polyelectrolytes and dyes were assembled onto MF particles by layer-by-layer adsorption in water according to the method reported previously.⁷⁻⁹ The first layer was deposited by the addition of 0.3 mL of MF particles to a 1.5-mL aliquot of a 1 mg mL⁻¹ aqueous PSS solution in 0.5 M NaCl, allowing 20 min for adsorption. The excess polyelectrolyte was removed by three repeated centrifugation (2000g, 4 min)/washing/redispersion cycles with water. The next layer of PAH or labeled PAH was deposited from 1 mg mL⁻¹ PAH in 0.5 M NaCl solution using the same procedure. Subsequent alternating PSS and PAH or labeled PAH layers were deposited in identical fashion until the desired number of multilayers was achieved. The amount of polyelectrolyte adsorbed onto the MF latex particles can be calculated using de Feijter's relation.¹⁴ The average amount adsorbed per PSS/PAH layer pair is $2.1 \times 0.7 \text{ mg m}^{-2}$.¹⁵

Hollow capsules were prepared by dissolving the core MF particles in HCl solution (pH = 1). The resulting hollow polymer capsules were then centrifuged at 2000g for 5 min, exposed to water again, washed an additional two times with water, and finally redispersed in water.

Low molecular weight dyes (TC, TCC, and IDCC) were deposited onto the surface of complementary charged preassembled capsules by the addition of dyes with desired concentrations into the (PSS/PAH)₄ capsule solution, allowing 20 min for adsorption. The resulting solutions were used directly for the titration experiments without any washing. For comparative studies, different light-harvesting capsules were fabricated by different combinations of dyes (Table 1)

SCHEME 2: Two Options for Energy-Transfer Directions

SCHEME 3: Molecular Structures of Dyes and Polyelectrolytes Used in the Experiments

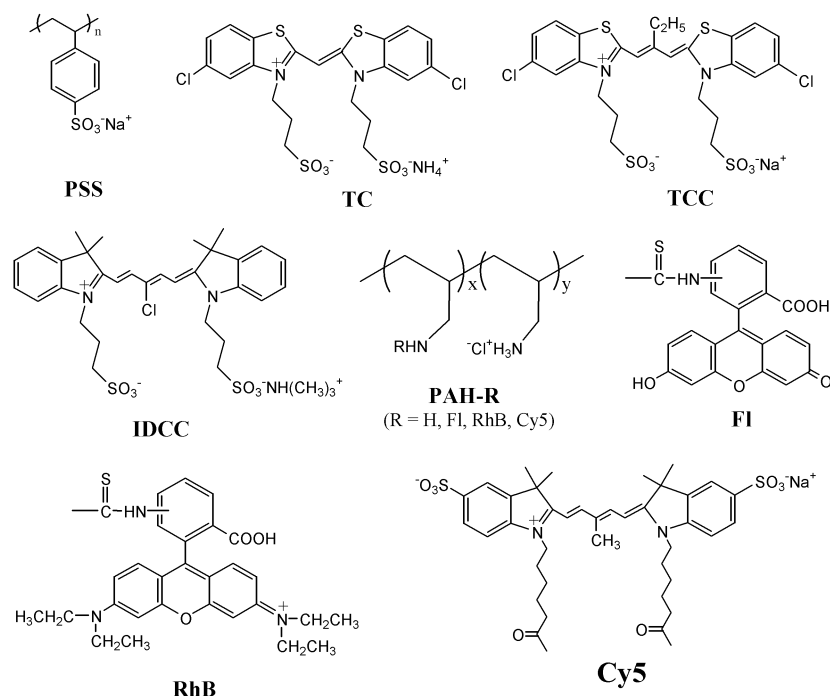


TABLE 1: Light-Harvesting Capsules (LHCap) with Different Combinations of Dyes

(PSS/PAH) ₄ /TC-TCC-IDCC	LHCap1a
PSS/PAH/IDCC/PAH/TCC/PAH/TC/PAH	LHCap1b
PSS/PAH/PSS/PAH-RhB/PSS/PAH-FI/PSS/PAH	LHCap2a
PSS/PAH-Cy5/PSS/PAH-RhB/PSS/PAH/PSS/PAH	LHCap2b
PSS/PAH-Cy5/PSS/PAH/PSS/PAH-FI/PSS/PAH	LHCap2c
PSS/PAH-Cy5/PSS/PAH-RhB/PSS/PAH-FI/PSS/PAH	LHCap2d
PSS/PAH/PSS/PAH-RhB/PSS/PAH/TC	LHCap3a
PSS/PAH-Cy5/PSS/PAH-RhB/PSS/PAH/PSS	LHCap3b
PSS/PAH-Cy5/PSS/PAH/PSS/PAH/TC	LHCap3c
PSS/PAH-Cy5/PSS/PAH-RhB/PSS/PAH/TC	LHCap3d

Confocal micrographs were taken with an Aristoplan confocal laser scanning microscope from Leica, equipped with a 100× oil-immersion objective and a numerical aperture of 1.4. The number of capsules was counted under a bright-line hemacytometer (Sigma).

Absorption spectra were measured using a Varian Cary 4E UV–visible spectrophotometer. The amount of each dye deposited into the capsules was determined by measurements of the absorption spectra of a hollow-capsule solution after diluting to a suitable concentration.

Fluorescence spectra were obtained using a Spex Fluorolog 1680 double-beam spectrometer. All measurements were performed on air-equilibrated solutions at room temperature. Typically, ca. 0.3 mL of the four-bilayer PSS/PAH hollow-capsule suspension was pipetted into 2.7 mL of water in a fluorimeter cell, and the dispersion was agitated for 0.5 min. The fluorescence spectrum of this dispersion was recorded and used as a background for subsequently measured spectra. An aliquot of the dye solution was then added, the dispersion was stirred for 2 min, and the fluorescence spectrum was recorded. This procedure was repeated to cover a range of dye concentrations, dye combinations, and dye ratios.

Quantitative values for the FRET can be obtained either by measuring the increase of the acceptor fluorescence or by measuring the quenching of the donor fluorescence. Both values were calculated by integrating the fluorescence intensity (I_f) over the energy ($\tilde{\nu}$), thus obtaining the relative number of emitted

light photons (N_i) for each step.

$$N_i = \int I_f d\tilde{\nu}$$

The fluorescence quantum yield $\phi = 0.38$ of TC J-aggregates adsorbed to PAH for an excitation wavelength of 402 nm is known from the literature.¹⁶ Hence, this value was taken as the standard for the quantum yield of the transferred or quenched energy. For each experiment with different dye combinations, the same amount of light was absorbed by the dye TC. Because of the high excess of TC, the added dyes TCC and IDCC absorb almost no additional photons at 410 nm. Therefore, the fluorescence quantum yield (ϕ_i) for each step can be calculated by the following equation:

$$\phi_i = \phi_0 \frac{N_i}{N_0}$$

where ϕ_0 and N_0 are the fluorescence quantum yield and the number of emitted photons of the adsorbed TC dye in the absence of TCC and IDCC under the excitation of 410-nm light, respectively. N_i was obtained by integrating the fluorescence spectrum of the corresponding dye over the energy.

Results and Discussion

In the presence of hollow capsules of (PSS/PAH)₄, the TC fluorescence intensity is approximately 40 times higher than that measured for the dye/water reference solution, indicating that there is strong electrostatic interaction between anionic dyes and PAH when PAH forms the outer layer. The charged sites of PAH available for dye adsorption cause the extraction of dye from the bulk solution to the surface of (PSS/PAH)₄ hollow capsules. But it has to be pointed out that the dye–PAH binding is not stronger than the PSS–PAH interaction. This can be proved by the fact that the addition of polyanion to multilayer films with prebound dye causes the removal of the dye because of the complexation of the polyelectrolyte species. Hence, the breaking of electrostatic interactions between the oppositely

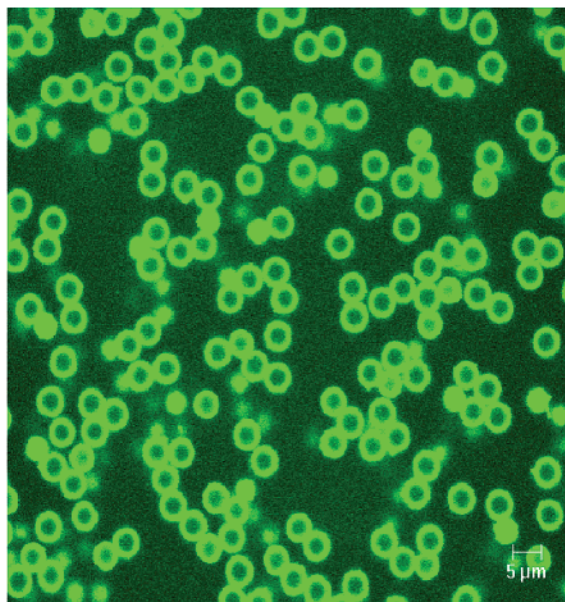


Figure 1. Confocal laser scanning microscopy (CLSM) image of hollow capsules of (PSS/PAH)₄ dispersed in the solution containing TC, TCC, and IDCC.

charged polyelectrolytes forming the multilayer films upon dye binding can be excluded.

The first system was constructed by means of two methods with three negatively charged TC (antenna), TCC (receiver and antenna), and IDCC (receiver). (i) The anionic cyanines were coadsorbed onto the surface of preassembled hollow capsules of (PSS/PAH)₄ with the PAH outermost layer, resulting in light-harvesting capsules of [(PSS/PAH)₄TC–TCC–IDCC] (LHCap1a). Figure 1 shows the confocal fluorescence micrograph of LHCap1a. We can see that the capsules possess a shape-persistent spherical hollow architecture in solution and that cyanines can enter the capsules by means of diffusion. Binding does not occur only in the outermost layer or in neighboring positive layers. It is known that binding occurs throughout the multilayer film.¹⁵ The largest fraction of cyanines is adsorbed on the shell wall. Quantification of this will be given later. (ii) The cyanines were assembled stepwise with PAH along the radial direction to obtain (PSS/PAH/IDCC/PAH/TCC/PAH/TC/PAH) (LHCap1b). But the ability of small molecules to permeate the polyelectrolyte layers probably did not allow the formation of ideal sandwich structures.¹⁷ Because the thickness of the single layer is around 1.3 nm,¹⁸ the energy transfer should be reasonably well-controlled by Förster transfer (Förster distance, 5.1 nm).¹⁹

A shift of the TC-monomer maximum absorption at 406 nm to 465 nm proves the formation of J-aggregates. In contrast, TCC and IDCC absorption spectra do not change upon adsorption onto the surface of the capsules, pointing to the existence of monomers. The absorption spectra of TC, TCC, and IDCC are completely separated from one another, permitting selective excitation of either dye (Figure 2a). The fluorescence emission spectra of TC and TCC have extensive overlap with the absorption spectra of TCC and IDCC, respectively. TC absorbs in the blue region of the visible spectrum, and the emission maximum of its J-aggregate, 485 nm, is coincident with the intense absorption band of TCC ($\lambda = 565$ nm). The TCC emission (590 nm) essentially overlaps with the absorption of IDCC (645 nm). Together, the three dyes are strongly absorbing between 350 and 700 nm. If the dyes are assembled close to each other, then the fluorescence from IDCC at 675

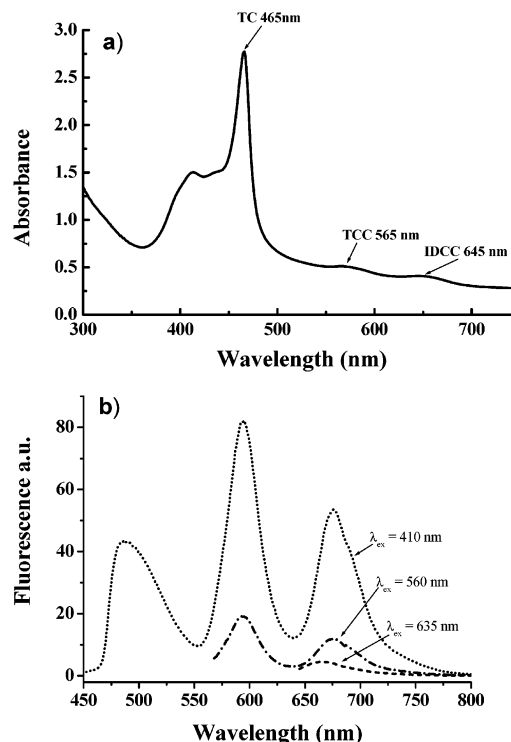


Figure 2. LHCap1a with three cyanine dyes (molar ratio of TC/TCC/IDCC = 83:1:1) coadsorbed onto the surface of preassembled eight-layer hollow capsules (PSS/PAH)₄. (a) Absorption spectra and (b) fluorescence spectra by selective excitation of TC at 410 nm, TCC at 560 nm, and IDCC at 635 nm.

nm can result from either direct excitation of IDCC in the red, from excitation of TCC in the green followed by energy-transfer step 2 to IDCC, from excitation of TC in the blue and direct energy-transfer step 3 to IDCC, or via the intermediacy of TCC (two-step 1 + 2, Scheme 2) (Figure 2b).

From fluorescence measurements, we can obtain direct information about these steps in LHCap1. The FRET process in a mixture of TC, TCC, and IDCC in solution is negligible. Also, at dye concentrations of less than 10^{-6} M, fluorescence self-quenching of monomeric dyes in solution can be ruled out. After addition of the capsules, dye molecules adsorb onto their surfaces, allowing FRET to occur. To examine the two-step (1 + 2) energy transfer TC → TCC → IDCC in some detail, three series of titration experiments were done with two dyes adsorbed on the surface of the capsules and the concentration of the third dye increasing gradually. For all experiments, an excitation wavelength of 410 nm was used, where the TC aggregate is strongly excited while TCC and IDCC are only very weakly excited.

In the first experiment, the IDCC concentration was varied from 0 to 3.0×10^{-6} M while the concentrations of both TC and TCC were kept constant at 5×10^{-5} and 6×10^{-7} M, respectively. Figure 3a shows the fluorescence spectra of capsules in the presence of different amounts of the acceptor IDCC. First, TC that was adsorbed to the capsules was excited with 410-nm light in the absence of TCC and IDCC. The fluorescence quantum yield is $\phi_f = 0.4$. After the addition of TCC, the fluorescence quantum yield of the TC J-aggregates is reduced to $\phi_f = 0.11$ at a dye ratio of TC/TCC = 83:1. Instead, the TCC shows strongly increased fluorescence of $\phi_f = 0.37$ although it is not directly excited. Interestingly, the total fluorescence quantum yield for both dyes is higher than that for the TC J-aggregates alone. This process can be described by fast coherent energy transfer within the J-aggregate of TC

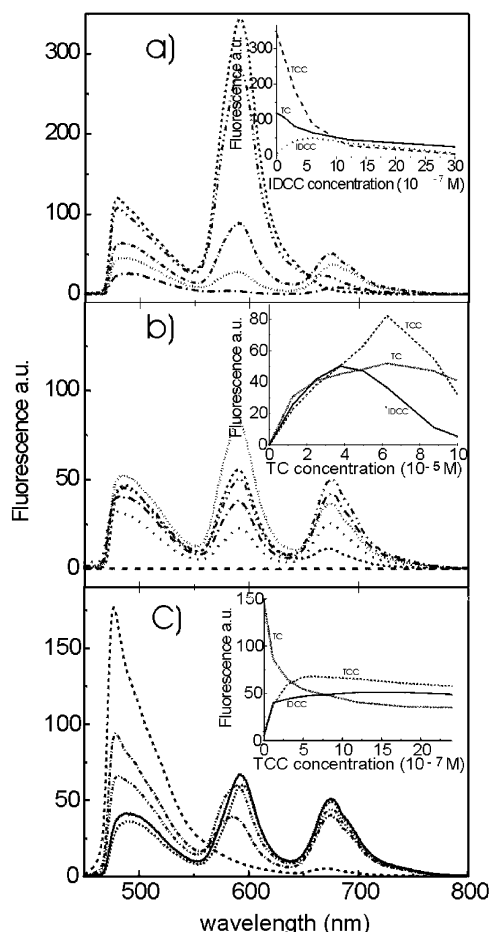


Figure 3. Fluorescence spectra ($\lambda_{\text{exc}} = 410$ nm) of LHCap1a with three cyanine dyes coadsorbed onto the surface of hollow capsules (PSS/PAH)₄. (a) IDCC concentrations were 0, 1.2×10^{-7} , 3×10^{-7} , 6×10^{-7} , 12×10^{-7} , and 30×10^{-7} M while the concentrations of both TC and TCC were kept constant at 5×10^{-5} and 6×10^{-7} M, respectively. (b) TC concentrations were 0, 1.25×10^{-5} , 3.75×10^{-5} , 5×10^{-5} , 6.25×10^{-5} , 8.75×10^{-5} , and 10×10^{-5} M while the concentrations of TCC and IDCC were kept constant at 6×10^{-7} M. (c) TCC concentrations were 0, 1.2×10^{-7} , 3×10^{-7} , 4.8×10^{-7} , 6×10^{-7} , 12×10^{-7} , 18×10^{-7} , and 24×10^{-7} M while the concentrations of TC and IDCC were kept constant at 5×10^{-5} and 6×10^{-7} M, respectively. The insets show the fluorescence intensities at 485, 590, and 675 nm as a function of the IDCC, TC, and TCC concentrations, respectively.

donor molecules followed by Förster transfer to the monomeric TCC acceptor molecules. If the J-aggregate is excited, then the energy can be transferred very efficiently to each point of the coherently coupled domain,²⁰ where a suitable quencher molecule such as TCC is located. This would increase the overall transfer rate for J-aggregate-to-monomer transfer by a factor of N because the dipole moment of an aggregate of N molecules is $N^{1/2}$ times the monomeric dipole moment.^{2c} The Förster transfer rate is proportional to the square of the dipole–dipole interaction, which results in N times faster transfer from an aggregate to a monomer than that between two monomers. The addition of IDCC leads to further quenching of the TC emission to a value of $\phi_{\text{H}} = 0.032$ and substantial quenching of the TCC emission by 82% to only $\phi_{\text{H}} = 0.061$. Simultaneously, the IDCC emission at 675 nm is switched on, but the quantum yield for its fluorescence is only $\phi_{\text{H}} = 0.031$. One has to take into account that this value is much higher than that obtained by selective excitation of TCC at 560 nm, even for direct excitation at 640 nm (Figure 2b). It is obvious that the higher fluorescence quantum yield of IDCC excited at 410 nm is due to two-step

energy transfer. Self-quenching at higher concentration above an IDCC concentration of 6×10^{-7} M reduces the energy transfer (inset of Figure 3a). The rate of quenching of TC with the concentration of IDCC is smaller than the rate of quenching of TCC. This could be the reason that the FRET step 2 $\text{TCC} \rightarrow \text{IDCC}$ proceeds efficiently under the excitation of TC.

In the second experiment, the TC concentration was varied from 0 to 1×10^{-4} M while the concentrations of both TCC and IDCC were kept constant at 6×10^{-7} M. In the absence of TC, the sum of the direct excitation of TCC and FRET 2 to IDCC as well as the direct excitation of IDCC yielded negligible fluorescence (Figure 3b). The addition of TC leads to the characteristic triple-peaked fluorescence, demonstrating efficient FRET from TC to TCC and IDCC. However, the fluorescence intensity of both TC and TCC (485 and 590 nm, respectively) reaches its maximum at 6.25×10^{-5} M TC whereas the IDCC fluorescence decreases at 3.75×10^{-5} M TC (inset of Figure 3b). Probably, IDCC with the longer polymethine chain is more unstable under irradiation and is partially destroyed during the titration experiments.

In the third experiment, the TCC concentration was varied from 0 to 2.4×10^{-6} M while optimal concentrations of TC (5×10^{-5} M) and IDCC (6×10^{-7} M) were taken according to the above results, respectively. IDCC is excited to a small extent, showing that direct FRET 3 takes place in the absence of TCC. Nevertheless, as the concentration of TCC increases, the fluorescence of IDCC is greatly enhanced, and that of TC is extensively quenched (Figure 3c). At the optimal concentration of TCC (6×10^{-7} M), the fluorescence of IDCC is 9 times higher than in absence of TCC. This clearly proves the two-step energy transfer 1 + 2. In addition, the strong quenching of the TCC fluorescence induced by FRET 1 in the presence of IDCC confirms this result very well. Hence, the main contribution of the IDCC fluorescence comes from the two step FRET pathway, illustrating that all three components are required to be present for the blue-light-activated energy cascade to function.

The above dye fluorescence–concentration curves can be explained as follows. The degree of FRET is dependent on the capsule surface area available for dye adsorption. In PSS/PAH multilayers, approximately 10–30% of the cationic sites of PAH are not utilized in ion-pair formation with adjacent PSS layers, and these sites provide a positively charged surface for the adsorption of the anionic dyes.¹⁵ At the corresponding optimal concentrations (TC, 5×10^{-5} M; TCC, 6×10^{-7} M; IDCC, 6×10^{-7} M), saturation binding of the charged sites within the polyelectrolyte multilayer film occurs. To assess the extent of TC, TCC, and IDCC binding below the corresponding saturation-binding concentration, (PSS/PAH)₄ hollow capsules were exposed to concentrations over the range of 0– 3.75×10^{-5} M for TC, 0– 6×10^{-7} M for TCC, and 0– 6×10^{-7} M for IDCC and were allowed to interact for 2 min, and the hollow capsules were then centrifuged. The supernatant was analyzed for free (unbound) dyes by fluorescence measurements. At all concentrations studied, the free-dye fluorescence intensity in the supernatant was less than 5% of that measured for dye/water reference solutions. This confirms that the fluorescence observed at concentrations below that of saturation binding is from bound dye.

Microscopy enabled the determination of the number of (PSS/PAH)₄ hollow capsules in each sample. Using these data and the corresponding optimal dye concentrations (TC, 5×10^{-5} M; TCC, 6×10^{-7} M; IDCC, 6×10^{-7} M) at which saturation coverage occurs, the maximum number of dye molecules per

TABLE 2: Fluorescence Quantum Yields (ϕ_f , $\lambda_{\text{exc}} = 410$ nm) of Different Combinations of TC, TCC, and IDCC

dyes	$\lambda_{\text{max}}^{\text{em}}$ (nm)	fluorescence quantum yield ϕ_f^a	fluorescence quantum yield ϕ_f^b
TC	485	0.4	0.4
TC + TCC	485, 590	0.11, 0.37	0.11, 0.25
TC + IDCC	485, 675	0.2, 0.004	0.11, 0.002
TCC + IDCC	no peak	0, 0	0, 0
TC + TCC + IDCC	485, 590, 675	0.032, 0.061, 0.031	0.026, 0.05, 0.0031

^aCombinations that have been coadsorbed onto the surface of preassembled eight-layer hollow capsules (PSS/PAH)₄ and with contrast dye concentrations of 5×10^{-5} M for TC, 6×10^{-7} M for IDCC, and 6×10^{-7} M for TCC. ^bCombinations that have been assembled stepwise with PAH along the radial direction.

100 nm² was determined to be approximately 1200 TC molecules, 15 TCC molecules, and 15 IDCC molecules. That means that an acceptor is expected within an area of 6.67 nm² around a donor. Hence the donor/acceptor distance amounts to $r = (6.67/\pi)^{1/2} = 1.46$ nm. Thus, we expect efficient energy transfer.

Quantitative fluorescence quantum yields of LHCap1a and 1b for different dye combinations are summarized in Table 2. As shown, two-step FRET occurs efficiently in LHCap1a where cyanines are coadsorbed in preassembled capsules. But the sequentially assembled LHCap1b has a lower FRET quantum yield. The main reason may be dye desorption commonly associated with constructing polyelectrolyte–dye multilayer structures by the stepwise adsorption of several oppositely charged species.²¹ It is also difficult to control the concentration ratio between the dyes. However, the method of incorporating dyes in preassembled multilayer films avoided these problems. In addition, the amount of the incorporated dye can be controlled by altering the PE multilayer film thickness.¹⁵ Two-step FRET occurs parallel to the surface of LHCap1a, but it is difficult to claim that two-step FRET occurs perpendicularly across the surface of LHCap1b because low molecular weight species can permeate PE layers and whether sandwich structures were obtained in reality remains questionable.

Therefore, a second system was constructed from a sequentially adsorbed sequence of the dye-labeled PAH (PAH–Cy5, PAH–RhB and PAH–FI) with intervening PSS layers and varying dye combinations in order to obtain the unidirectional FRET perpendicularly across the wall. Four kinds of capsules, including (PSS/PAH/PSS/PAH–RhB/PSS/PAH–FI/PSS/PAH) (LHCap2a), (PSS/PAH–Cy5/PSS/PAH–RhB/PSS/PAH/PSS/PAH) (LHCap2b), (PSS/PAH–Cy5/PSS/PAH/PSS/PAH–FI/PSS/PAH) (LHCap2c), and (PSS/PAH–Cy5/PSS/PAH–RhB/PSS/PAH–FI/PSS/PAH) (LHCap2d), were fabricated by the layer-by-layer self-assembly technique (Table 1). Figure 4 shows composite absorption and emission spectra of this system. After deposition onto the surface, PAH–FI, PAH–RhB, and PAH–Cy5 show red shifts of 7, 10, and 10 nm, respectively, suggesting that strong electrostatic interactions between PSS and labeled PAH occur. Decher and co-workers reported that unbranched polyelectrolytes such as PAH and PSS interpenetrate substantially when they are sequentially adsorbed.^{7a} A wavelength of 460 nm was used for the excitation of the second system. At this wavelength, the absorbance of PAH–FI is rather high whereas that of both PAH–RhB and PAH–Cy5 is very low. The FRET PAH–FI \rightarrow PAH–RhB (step 1)²² works well in LHCap2a. The fluorescence spectrum of LHCap2b in the absence of PAH–FI exhibits a small fluorescence maximum at 590 nm for PAH–RhB and almost no fluorescence at 676 nm for PAH–Cy5. However, in the absence of PAH–RhB, the

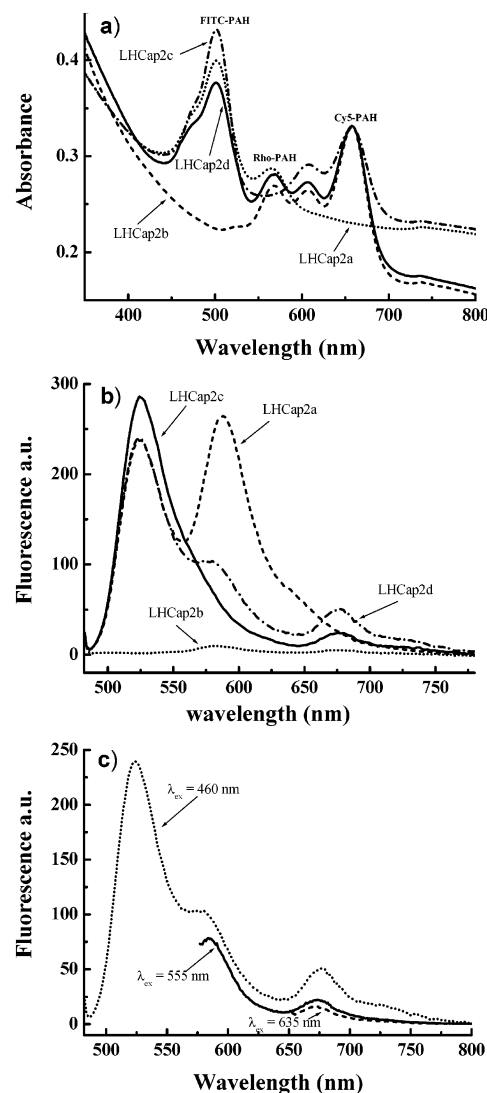


Figure 4. (a) UV–vis absorption and (b) fluorescence spectra ($\lambda_{\text{exc}} = 460$ nm) of the second system including eight-layer hollow capsules LHCap2a, LHCap2b, LHCap2c, and LHCap2d. (c) Fluorescence spectra of LHCap2d after selective excitation of FI at 460 nm, RhB at 555 nm, and Cy5 at 635 nm.

emission of PAH–Cy5 is observed by exciting into the fluorescein absorption band. This is evidence of direct energy-transfer PAH–FI \rightarrow PAH–Cy5 (step 3) in LHCap2c, although it is not efficient. In LHCap2d, there is quenching of the PAH–FI emission at 524 nm, substantial quenching of the PAH–RhB emission at 590 nm, and enhanced PAH–Cy5 emission at 676 nm relative to the reference spectra of LHCap2a, LHCap2b, and LHCap2c. The fluorescence intensity of Cy5 under the excitation of fluorescein at 460 nm is much higher than that after the selective excitation of rhodamine at 555 nm or cyanine at 635 nm (Figure 4c). Therefore, it is obvious that a two-step energy-transfer cascade PAH–FI \rightarrow PAH–RhB \rightarrow PAH–Cy5 occurs along the radial direction of capsules under the excitation of PAH–FI. Sufficient excited-state energy of PAH–RhB induced by FRET step 1 enables the FRET step 2 from PAH–RhB to PAH–Cy5. Thus, PAH–RhB acts as the bridge for downhill energy transfer from PAH–FI to PAH–Cy5. However, the energy transfer to Cy5 from the donor and the bridge is less efficient than in the first system.

To improve the unidirectional FRET, a third system, including capsules of (PSS/PAH/PSS/PAH–RhB/PSS/PAH/TC) (LHCap3a), (PSS/PAH–Cy5/PSS/PAH–RhB/PSS/PAH/PSS)

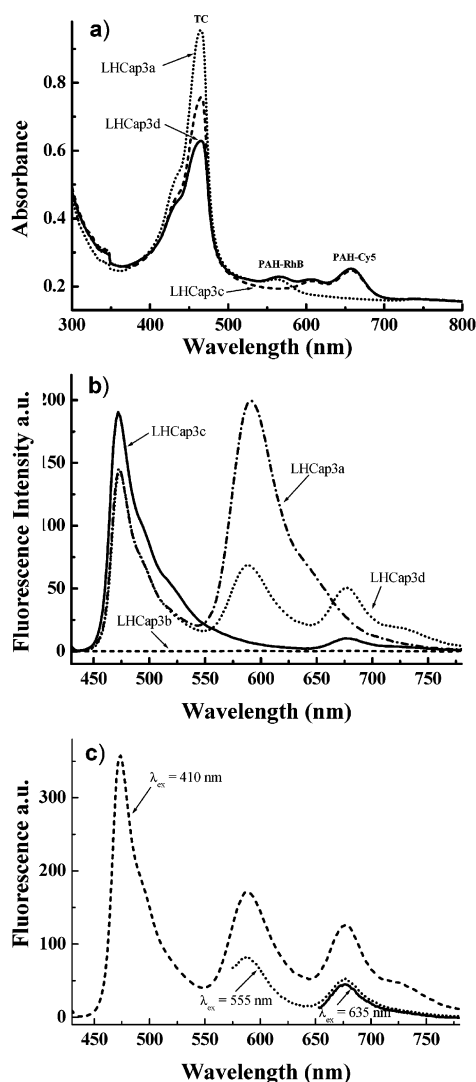


Figure 5. (a) UV-vis absorption and (b) fluorescence spectra ($\lambda_{ex} = 410$ nm) of the third system including seven-layer hollow capsules LHCap3a, LHCap3b, LHCap3c, and LHCap3d. (c) Fluorescence spectra of LHCap3d after the selective excitation of TC at 410 nm, RhB at 555 nm, and Cy5 at 635 nm.

(LHCap3b), (PSS/PAH-Cy5/PSS/PAH/PSS/PAH/TC) (LHCap3c), and (PSS/PAH-Cy5/PSS/PAH-RhB/PSS/PAH/TC) (LHCap3d), was fabricated as the second system but by replacing PAH-FI with the J-aggregate of TC (Table 1). Figure 5 shows absorption and fluorescence spectra for LHCap3 with different combinations of PAH-Cy5, PAH-RhB, and TC obtained by excitation of TC ($\lambda_{ex} = 410$ nm). Irradiation at 410 nm results in the strong fluorescence of TC J-aggregates at 472 nm in the absence of PAH-RhB and PAH-Cy5. The intense J band of TC permits the energy transfer from TC \rightarrow PAH-RhB in LHCap3a to proceed very efficiently. In the absence of TC, neither PAH-RhB nor PAH-Cy5 shows visible fluorescence (LHCap3b). The TC energy can be transferred to PAH-Cy5 via step 3, but this way is not efficient compared to energy transfer from TC to PAH-RhB (LHCap3c). LHCap3d has the same absorbance at 658 nm as LHCap3c and lower absorbance than both LHCap3a and LHCap3c at 465 nm; it shows higher fluorescence intensity at 675 nm under the excitation of TC relative to the reference spectra of LHCap3a, LHCap3b, and LHCap3c. Maybe the intense and broad J band of TC permits the excited TC to transfer energy efficiently either to PAH-RhB or to PAH-Cy5, and the excited PAH-RhB can further transfer energy to PAH-Cy5. The fluorescence spectra of

LHCap3d obtained by the selective excitation provide additional proof for two-step FRET (Figure 5c). Similar to that of LHCap 1 and 2, the excitation of TC at 410 nm results in much stronger fluorescence than the excitation of rhodamine at 555 nm and cyanine at 635 nm.

Comparison of the LHCap 1, 2, and 3 systems shows that the two-step energy transfer of the first and third systems is more efficient than that of the second system. This result strongly suggests that the J-aggregates as the elementary excitation unit are better suited for light-harvesting systems than single dye molecules. An open question is the size of the coherently coupled aggregate, which can be answered by temperature-dependent measurements of the FRET in these capsule systems.

Conclusions

The elementary energy-transfer steps mimicking photosynthesis have been discussed with complementary dyes assembled onto the surface of capsules. The flow of the excitation energy could be manipulated parallel to the capsule surface by coadsorbing dyes to preassembled PSS/PAH multilayer films or perpendicularly across the wall by layering dyes along the radial direction. Generally, the smaller dimensionality of the FRET in the radial arrangement reduces the efficiency. The less-efficient radial energy transfer could be improved by means of an optimized combination of antenna dyes and by the utilization of J-aggregates. The antenna dyes harvest the light energy and conduct it downhill by FRET from the exterior to the interior of the capsules, where photochemical initiators or semiconductor nanoparticles could induce chemical reactions. Our prepared light-harvesting capsules show some analogy to the chloroplasts in nature. But the efficiency up to now is much smaller.

In summary, the utilization of biology-based ideas and principles to the design of artificial photosynthetic nanostructures opens the door to research and applications in the information technology and biological realms. Future efforts will be directed toward optimizing the energy-transfer efficiencies through variation of the actual components to adjust the electronic coupling and distances between donors and acceptors according to the requirements of FRET. Taking the light-harvesting system of nature as a model, the formation of aggregates of all three dyes may further improve the FRET.

Acknowledgment. This work was partly supported by the BASF and BMBF, grant 03C0293A1, as well as the Funds of the Chemical Industry.

References and Notes

- (1) (a) Larkum, A. W. D.; Barrett, J. *Adv. Bot. Res.* **1983**, *10*, 1-219. (b) *Photosynthetic Light-Harvesting Systems*; Scheer, H.; Siegried, S., Eds.; W. de Gruyter: Berlin, 1988. (c) Mauzerall, D. C.; Greenbaum, N. L. *Biochim. Biophys. Acta* **1989**, *974*, 119-140. (d) Gust, D.; Moore, T. A.; Moore, A. L.; Lee, S.-J.; Bittersman, E.; Juttrull, D. K.; Rehms, A. A.; DeGraziano, J. M.; Ma, X. C.; Gao, F.; Belford, R. E.; Trier, T. T. *Science (Washington, D.C.)* **1990**, *248*, 199.
- (2) (a) McDermott, G.; Prince, S. M.; Freer, A. A.; Haworthornthwaite-Lawless, A. M.; Papiz, M. Z.; Cogdell, R. J.; Isaacs, N. W. *Nature (London)* **1995**, *374*, 517-521. (b) Karrasch, S.; Bullough, P. A.; Ghosh, R. *EMBO J.* **1995**, *14*, 631-638. (c) Pullerits, T.; Sundström, V. *Acc. Chem. Res.* **1996**, *29*, 381-389. (d) Gust, D.; Moore, T. A.; Moore, A. L. *Acc. Chem. Res.* **2001**, *34*, 40.
- (3) (a) Borisov, A. Yu.; Freiberg, A. M.; Godik, V. I.; Rebane, K. K.; Timpmann, K. K. *Biochim. Biophys. Acta* **1985**, *807*, 221. (b) Sundström, V.; Van Grondelle, R.; Bergström, H.; Åkesson, E.; Gillbro, T. *Biochim. Biophys. Acta* **1986**, *851*, 431.
- (4) (a) Kaschak, D. M.; Lean, J. T.; Waraksa, C. C.; Saupe, G. B.; Usami, H.; Mallouk, T. E. *J. Am. Chem. Soc.* **1999**, *121*, 3435. (b) Scholes,

- G. D. *J. Phys. Chem.* **1996**, *100*, 18731. (c) Scholes, G. D.; Jordanides, X. J.; Fleming, G. R. *J. Phys. Chem. B* **2001**, *105*, 1640.
- (5) (a) Wasielewski, M. R. *Chem. Rev.* **1992**, *92*, 435. (b) Watkins, D. M.; Fox, M. A. *J. Am. Chem. Soc.* **1996**, *118*, 4344. (c) Fossum, R. D.; Fox, M. A. *J. Am. Chem. Soc.* **1997**, *119*, 1197. (d) Dupray, L. N.; Devenney, M.; Striplin, D. R.; Meyer, T. J. *J. Am. Chem. Soc.* **1997**, *119*, 10243. (e) Balzani, V.; Campagna, S.; Denti, G.; Juris, A.; Serroni, S.; Venturi, M. *Acc. Chem. Res.* **1998**, *31*, 26.
- (6) (a) Haycock, R. A.; Yartsev, A.; Michelsen, U.; Sundström, V.; Hunter, C. A. *Angew. Chem., Int. Ed.* **2000**, *39*, 3616–3619. (b) Miyatake, T.; Tamiaki, H.; Holzwarth, A. R.; Schaffner, K. *Helv. Chim. Acta* **1999**, *82*, 797–811. (c) Yu, L.; Lindsey, J. S. *J. Org. Chem.* **2001**, *66*, 7402. (d) King, B. A.; Winter, A.; McAnney, T. B.; Boxer, S. G. *J. Phys. Chem. B* **2001**, *105*, 1856.
- (7) (a) Decher, G. *Science (Washington, D.C.)* **1997**, *277*, 1232. (b) Donath, E.; Sukhorukov, G. B.; Caruso, F.; Davis, S. A.; Möhwald, H. *Angew. Chem., Int. Ed.* **1998**, *37*, 2202. (c) Caruso, F.; Caruso, R.; Möhwald, H. *Science (Washington, D.C.)* **1998**, *282*, 1111. (d) Dai, Z. F.; Dähne, L.; Möhwald, H.; Tiersch, B. *Angew. Chem., Int. Ed.* **2002**, *41*(21).
- (8) (a) Ibarz, G.; Dähne, L.; Donath, E.; Möhwald, H. *Adv. Mater. (Weinheim, Ger.)* **2001**, *13*, 1324–1327. (b) Loporatti, S.; Gao, C.; Voigt, A.; Donath, E.; Möhwald, H. *Eur. Phys. J. E* **2001**, *5*, 13–20. (c) Moya, S.; Donath, E.; Sukhorukov, G. B.; Auch, M.; Bäuml, H.; Lichtenfeld, H.; Möhwald, H. *Macromolecules* **2000**, *33*, 4538–4544. (d) Möhwald, H.; Lichtenfeld, H.; Moya, S.; Voigt, A.; Bäuml, H.; Sukhorukov, G.; Caruso, F.; Donath, E. *Macromol. Symp.* **1999**, *145*, 75. (e) Antipov, A. A.; Sukhorukov, G. B.; Donath, E.; Möhwald, H. *J. Phys. Chem. B* **2001**, *105*, 2281–2284.
- (9) (a) Dai, Z.; Voigt, A.; Loporatti, S.; Donath, E.; Dähne, L.; Möhwald, H. *Adv. Mater.* **2001**, *13*, 1339. (b) Dai, Z.; Voigt, A.; Donath, E.; Möhwald, H. *Macromol. Rapid Commun.* **2001**, *22*, 756. (c) Dai, Z.; Donath, E.; Dähne, L.; Möhwald, H. *Langmuir* **2002**, *18*, 4553–4555.
- (10) (a) Hess, S.; Visscher, K. J.; Pullerits, T.; Sundström, V.; Fowler, G. J. S.; Hunter, C. N. *Biochemistry* **1994**, *33*, 8300. (b) Pullerits, T.; Monshouwer, R.; van Mourik, F.; van Grondelle, F. *Chem. Phys.* **1995**, *194*, 395. (c) Reddy, N. R. S.; Picorel, R.; Small, G. J. *J. Phys. Chem.* **1992**, *96*, 6458.
- (11) (a) Dai, Z. F.; Peng, B. X. *Dyes Pigm.* **1998**, *36*, 169. (b) Dai, Z. F.; Peng, B. X. *Dyes Pigm.* **1998**, *36*, 243.
- (12) (a) Kometani, N.; Nakajima, H.; Asami, K.; Yonezawa, Y.; Kajimoto, O. *J. Phys. Chem. B* **2000**, *104*, 9630. (b) Dai, Z.; Peng, B.; Fang, L.; Y. J. *Chin. Chem. Soc. (Taipei)* **1998**, *45*, 643–648. (c) Dai, Z.; Lin, G.; Peng, B.; Li, Z. *Imaging Sci. J.* **1998**, *46*, 73–80. (d) Dai, Z.; Peng, B.; Chen, X. *Dyes Pigm.* **1999**, *40*, 219–223. (e) Dai, Z.; Peng, B.; Yang, Q.; Liu, S.; Ye, P. *Chem. Phys. Lett.* **2000**, *317*, 9–12. (f) Guan, J.; Dai, Z.; Tong, C.; Peng, B. *J. Fluoresc.* **2000**, *10*, 21–26. (g) Guan, J.; Dai, Z.; Tong, C.; Peng, B. *J. Photochem. Photobiol., A* **1998**, *114*, 45–49.
- (13) (a) Dai, Z. F.; Zastrow, H.; Loporatti, S.; Donath, E.; Möhwald, H.; Peng, B. X. *J. Dispersion Sci. Technol.* **2002**, *23*, 555–562. (b) Kaschak, D. M.; Mallouk, T. E. *J. Am. Chem. Soc.* **1996**, *118*, 4222–4223. (c) Della, C. L.; Gringnani, A.; Cassullo, M.; Caputo, G. WO Patent 97/13810, 1997.
- (14) de Feijter, J. A.; Benjamins, J.; Veer, F. A. *Biopolymers* **1978**, *17*, 1759.
- (15) Caruso, F.; Lichtenfeld, H.; Donath, E.; Möhwald, H. *Macromolecules* **1999**, *32*, 2317–2328.
- (16) Peyratout, C.; Donath, E.; Dähne, L. *Photochem. Photobiol. Sci.* **2002**, *1*, 87–91.
- (17) (a) Dai, Z. F.; Möhwald, H. *Chem.—Eur. J.* **2002**, *8*, 4751–4755. (b) Caruso, F.; Donath, E.; Möhwald, H. *J. Phys. Chem. B* **1998**, *102*, 2011–2016.
- (18) Loporatti, S.; Voigt, A.; Mitlöhner, R.; Sukhorukov, G.; Donath, E.; Möhwald, H. *Langmuir* **2000**, *16*, 4059–4063.
- (19) Chen, R.; Knutson, J. *Anal. Biochem.* **1988**, *172*, 61.
- (20) (a) Fidler, H.; Knoester, J.; Wiersma, D. A. *J. Phys. Chem.* **1991**, *95*, 7880. (b) Borja, M.; Dutta, P. K. *Nature (London)* **1993**, *362*, 43.
- (21) (a) Ariga, K.; Lvov, Y.; Kunitake, T. *J. Am. Chem. Soc.* **1997**, *119*, 2224. (b) Linford, M.; Auch, M.; Möhwald, H. *J. Am. Chem. Soc.* **1998**, *120*, 178.
- (22) (a) Gao, C.; Moya, S.; Lichtenfeld, H.; Casoli, A.; Fiedler, H.; Donath, E.; Möhwald, H. *Macromol. Mater. Eng.* **2001**, *286*, 355. (b) Klitzing, R.; Möhwald, H. *Macromolecules* **1996**, *29*, 6901–6906.